optica

Bloch oscillation and unidirectional translation of frequency in a dynamically modulated ring resonator

Luqi Yuan and Shanhui Fan*

Department of Electrical Engineering and Ginzton Laboratory, Stanford University, Stanford, California 94305, USA
**Corresponding author: shanhui@stanford.edu*

Received 7 July 2016; revised 14 August 2016; accepted 16 August 2016 (Doc. ID 270007); published 6 September 2016

The ability to control the spectrum of light is of fundamental significance in many applications of light. We consider a dynamically modulated ring resonator that supports a set of resonant modes equally spaced in their resonant frequencies, and is modulated at a frequency that is slightly detuned from the modal frequency spacing. We find that such a system can be mapped into a tight-binding model of photons under a constant effective force, and, as a result, the system exhibits Bloch oscillation along the frequency axis. The sign of the detuning is mapped to the sign of the effective force and hence controls the direction of the Bloch oscillation. We also show that a periodic switching of the detuning can lead to unidirectional transport of light along the frequency axis. Our work points to a new capability for manipulating the frequencies of light using dynamic microcavity structures.

OCIS codes: (230.5750) Resonators; (060.2630) Frequency modulation; (130.7405) Wavelength conversion devices.

http://dx.doi.org/10.1364/OPTICA.3.001014

1. INTRODUCTION

Microring resonators have been extensively used for explorations of fundamental physics and in a wide range of applications including spectroscopy, sensing, and information processing [1–5]. In particular, the resonant modes of a ring cavity form a frequency comb, and hence the ring can be used as the basis for compact and robust frequency comb sources [6–8]. In addition, active modulation of microring cavities can couple these resonant modes together, leading to new possibilities for manipulating the spectrum of light [9–11].

In the absence of group velocity dispersion in the ring waveguide, a ring cavity supports an equally spaced frequency comb [6]. In the *on-resonance modulation case*, in which the modulation frequency Ω is chosen to be equal to the frequency spacing Ω_R between the resonant modes in the comb, the system exhibits photonic transition [12–14] and can be mapped into a tight-binding model with each mode corresponding to one lattice site in the model [15,16]. Building upon this notion, in this paper we consider the *off-resonance modulation case*, in which the modulation frequency is slightly different from the frequency spacing. We show that, in such a case, the system can be mapped into a tight-binding model subject to a constant effective force for photons. Thus, the photon wave amplitudes in the system undergo Bloch oscillation along the frequency axis. Moreover, we find that a unidirectional transport of the light along the frequency axis can be achieved by periodically changing the modulation frequency Ω.

The Bloch oscillation of light has been previously explored in waveguide or waveguide array systems, with the oscillation occurring either in the spatial [17–21] or the spectral domain [22,23]. Our work here points to a novel manifestation of the effect of Bloch oscillation [24,25] and establishes a connection between the physics of microresonators and the physics of coherent dynamics of quantum particles under an external field. Moreover, the ability to achieve unidirectional transport of light along the frequency axis naturally leads to the capability of photon frequency translation, which is of interest for both classical and quantum information processing [26–28].

2. THEORETICAL ANALYSIS

To illustrate the essential physics, we first consider a simple physical model of a ring resonator undergoing dynamic refractive index modulation (Fig. 1). Suppose the waveguide forming the ring has no group velocity dispersion; the frequency of the mth resonant mode is then located at

$$\omega_m = \omega_0 + m\Omega_R, \tag{1}$$

where Ω_R is the free spectral range. Suppose we place an electro-optic modulator into the ring, with a modulation frequency $\Omega \approx \Omega_R$. A simple Hamiltonian for this system is then

$$H = \sum_m \omega_m a_m^\dagger a_m + \sum_m 2g\cos(\Omega t)(a_m^\dagger a_{m+1} + a_{m+1}^\dagger a_m), \tag{2}$$

where $a_m^\dagger$ and a_m are the creation and annihilation operators, respectively, for the mth resonant mode in the resonator. g is the

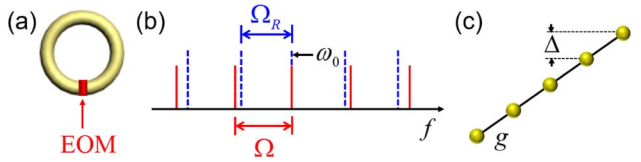

Fig. 1. (a) Ring resonator modulated by an electro-optic modulator (EOM). (b) In the absence of group velocity dispersion, the ring in (a) supports a set of resonant modes (blue dashed lines) with their resonant frequencies equally spaced by Ω_R. The modulation frequency Ω is chosen to be slightly different from Ω_R. For the modes that are located at ω_0, the modulation generates sidebands that are detuned from the other resonant modes. (c) The system as described in (b) can be mapped onto a tight-binding model of a photon under an effective force [Eq. (4)].

strength of modulation. We assume that the modes are all nondegenerate, and there is no backscattering in the waveguide forming the ring. Defining $c_m \equiv a_m e^{-i\omega_m t}$ and taking the rotating wave approximation, which is valid since $\Omega \approx \Omega_R$, we transform H in Eq. (2) to

$$H_{\mathrm{RWA}} = g\sum_m (e^{-i\Delta t} c_m^\dagger c_{m+1} + e^{i\Delta t} c_{m+1}^\dagger c_m), \tag{3}$$

where $\Delta \equiv \Omega - \Omega_R$ is the detuning. Equation (3) is equivalent to a time-independent Hamiltonian describing a photon in a one-dimensional lattice under a constant effective force:

$$\tilde{H}_{\mathrm{RWA}} = g\sum_m (c_m^\dagger c_{m+1} + c_{m+1}^\dagger c_m) + \sum_m m\Delta c_m^\dagger c_m, \tag{4}$$

as can be seen with the gauge transformation [29]

$$|\Psi\rangle = \sum_m v_m c_m^\dagger |0\rangle \to |\tilde{\Psi}\rangle = \sum_m \tilde{v}_m c_m^\dagger |0\rangle = \sum_m v_m e^{-im\Delta t} c_m^\dagger |0\rangle, \tag{5}$$

with $v_m(\tilde{v}_m)$ being the amplitude of the field at the mth mode. $|\Psi(\tilde{\Psi})\rangle$ satisfies the Schrödinger equation, $i(\partial/\partial t)|\Psi(\tilde{\Psi})\rangle = H_{\mathrm{RWA}}(\tilde{H}_{\mathrm{RWA}})|\Psi(\tilde{\Psi})\rangle$. In Eq. (4), we note that the frequency of the mode at the mth site is proportional to m, signifying the presence of a constant force, as schematically represented in Fig. 1(c). The strength of the effective force is $F = |\Delta/\Omega_R|$, which leads to a Bloch oscillation with a period $T_B = 2\pi/\Delta$ [24,30].

We now proceed with a more realistic model of a ring under dynamic modulation [16,31]. We expand the electric field inside the resonator as [32]

$$E(t, r_\perp, z) = \sum_m \mathcal{E}_m(t, z) E_m(r_\perp) e^{i\omega_m t}, \tag{6}$$

where z denotes the propagation direction along the waveguide that forms the ring resonator, $r_\perp$ gives the directions perpendicular to z, and $E_m(r_\perp)$ is the modal profile. $\mathcal{E}_m(t, z)$ is the modal amplitude for the mth resonant mode, which satisfies the following equation:

$$\left(\frac{\partial}{\partial z} + i\beta(\omega_m)\right)\mathcal{E}_m(t, z) - \frac{n_g(\omega_m)}{c}\frac{\partial}{\partial t}\mathcal{E}_m(t, z) = 0, \tag{7}$$

as can be derived from Maxwell's equations under the slowly varying envelope approximation. Here β is the wavevector in the z direction and n_g is the group index. The geometry of the ring imposes a periodic boundary condition $\mathcal{E}_m(t, z + L) = \mathcal{E}_m(t, z)$, where L is the circumference of the ring.

The electric field inside the resonator undergoes a dynamic phase modulation when it passes through an electro-optic phase modulator located at z_0, as described by

$$E(t^+, r_\perp, z_0) = E(t^-, r_\perp, z_0) e^{i\alpha \cos(\Omega t)}, \tag{8}$$

where α is the modulation amplitude and $t^\pm = t + 0^\pm$. The modulator imposes an additional time-dependent phase as the field passes through the modulator. We then use the rotating wave approximation to describe this process in terms of $\mathcal{E}_m(t, z)$ and obtain [33]

$$\begin{aligned}\mathcal{E}_m(t^+, z_0) = {} & J_0(\alpha)\mathcal{E}_m(t^-, z_0) \\ & + \sum_q i^q J_q(\alpha)[\mathcal{E}_{m+q}(t^-, z_0) e^{-iq\Delta t^-} \\ & + \mathcal{E}_{m-q}(t^-, z_0) e^{iq\Delta t^-}],\end{aligned} \tag{9}$$

where $\Delta = \Omega - \Omega_R$ and J_q is the Bessel function of the qth order.

To relate the physical model here to the simple model of Eq. (2), we keep only the coupling between nearest neighbor sidebands in Eq. (9), (i.e., keep only $q = \pm 1$ terms), and also assume that $J_0(\alpha) \approx 1$ and $J_1(\alpha) \approx \alpha/2$, which are valid in the weak modulation limit $\alpha \to 0$. Therefore, the variation of $\mathcal{E}_m$ in Eq. (9) after it passes the modulator is

$$\Delta\mathcal{E}_m(t, z_0) = i\frac{\alpha}{2}[\mathcal{E}_{m+1}(t, z_0) e^{-i\Delta t} + \mathcal{E}_{m-1}(t, z_0) e^{i\Delta t}]. \tag{10}$$

The total change of $\mathcal{E}_m$ over the propagation over one loop is $\mathcal{E}_m(t + T_R) = \mathcal{E}_m(t) + \Delta\mathcal{E}_m(t)$, where T_R is the round-trip propagation time around the ring [34]. By defining $\mathcal{E}_m(t + T_R) - \mathcal{E}_m(t) \equiv T_R \frac{\partial \mathcal{E}_m(T)}{\partial T}$, we obtain

$$T_R \frac{\partial \mathcal{E}_m}{\partial T} = i\frac{\alpha}{2}(\mathcal{E}_{m+1} e^{-i\Delta T} + \mathcal{E}_{m-1} e^{i\Delta T}). \tag{11}$$

We therefore see that, in the appropriate limit, Eqs. (7) and (9) describe a dynamics that is the same as the dynamics of the Hamiltonian of Eq. (2). Therefore, a ring under modulation can indeed exhibit Bloch oscillation physics in the frequency domain as described in Eq. (2).

3. NUMERICAL DEMONSTRATIONS OF BLOCH OSCILLATION AND TRANSLATION OF FREQUENCY

As a numerical confirmation of the analytical argument above, we solve Eqs. (7) and (9) to obtain the solution of the propagation of the electric field inside a ring resonator modulated by an electro-optic modulator (with $\alpha = 0.2$), without making the approximation that led to Eq. (10) [16]. The simulation involves solving for the dynamics for a finite set of modes around ω_0 as labeled by m. Let $n_0 = n(\omega_m)$ denote the effective refractive index for all resonant modes, so we have $\Omega_R = 2\pi\, c/n_0 L$. We inject the excitation into the system at the position z_s by the equation

$$\mathcal{E}_m(t^+, z_s) = \mathcal{E}_m(t^-, z_s) + S_m(t^-). \tag{12}$$

Here we assume that the excitation source is inside the ring. Throughout the paper, we choose

$$S_m(t) = f_m e^{-2\ln 2(t-20)^2/100}, \tag{13}$$

where t is in the unit of $n_0 L/c$. Here S_m is a pulse with its frequency centered at ω_m and its full width at half-maximum (FWHM) $\Delta\omega \ll \Omega_R$. f_m is the peak excitation amplitude for the mth mode. A given S_m essentially excites only the mth mode.

In the first set of simulations, for the excitation, we choose $f_0 = 1$ and $f_{m\neq 0} = 0$ in Eq. (13). We consider two modulation frequencies corresponding to detunings $\Delta = 0.1\ c/n_0L$ and $\Delta = 0.5\ c/n_0L$. In the simulation we include 17 resonant modes labeled with $m = -8, \ldots, 8$. We plot in Fig. 2 the temporal evolution of the total energy for each resonant mode ($I_m(t) \equiv \int_{\text{ring}} |\mathcal{E}_m(t,z)|^2 dz$). With a small detuning of $\Delta = 0.1\ c/n_0L$, we see the regular Bloch oscillation in the frequency dimension with the period $T_B = 20\pi\ n_0L/c$. When the detuning is large ($\Delta = 0.5\ c/n_0L$), we no longer observe the spectral Bloch oscillation because the modulation cannot couple the nearby resonant modes efficiently.

In Fig. 2(a), we observe that the oscillation pattern is symmetric around the $m = 0$ axis, in spite of the fact that the choice of $\Delta \neq 0$ gives a directional effective force along the frequency axis, as seen in Eq. (4). This effect was analytically studied in [35]. Physically, the excitation of a single site corresponds to a uniform excitation over the entire band in k_f-space (where k_f is the wavevector reciprocal to the frequency axis). The application of a force shifts the entire band and, hence, cannot create an asymmetric oscillation.

To observe an asymmetric Bloch oscillation pattern, we now consider an excitation profile by setting

$$f_m = \exp[-(\omega_m - \omega_c)^2/(5\Omega_R)^2], \tag{14}$$

in Eq. (13) with $\omega_c = \omega_0$. We again perform the simulation including 17 resonant modes. We consider the cases with the positive detuning $\Delta = 0.055\ c/n_0L$ and the negative detuning $\Delta = -0.055\ c/n_0L$, respectively. The total energy for each mode $I_m(t)$ is shown in Fig. 3. Unlike the case of Fig. 2, here the oscillation pattern no longer has a mirror symmetry around the $m = 0$ axis. The Gaussian excitation profile [Eq. (14)] excites only a portion of the band around $k_f = 0$. The effective force can then directionally shift the field amplitude profile in the k_f space as well as the frequency space. Changing the sign of the detuning Δ flips the oscillation pattern with respect to the $m = 0$ axis.

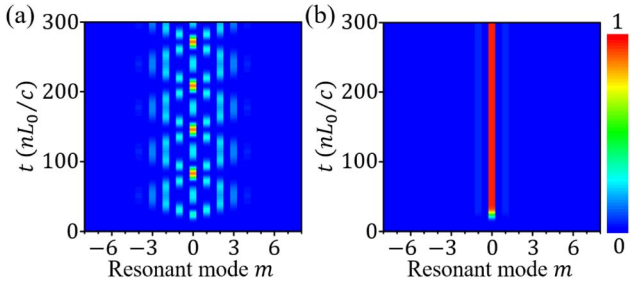

Fig. 2. Evolution in time of the total energy for each resonant mode ($I_m(t) \equiv \int_{\text{ring}} |\mathcal{E}_m(t,z)|^2 dz$): (a) $\Delta = 0.1\ c/n_0L$, and (b) $\Delta = 0.5\ c/n_0L$, when only the $m = 0$ mode is excited.

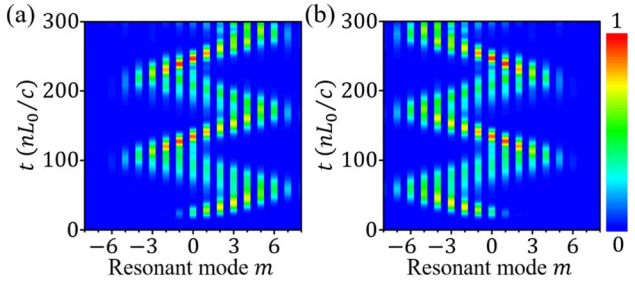

Fig. 3. Evolution in time of the total energy for each resonant mode ($I_m(t) \equiv \int_{\text{ring}} |\mathcal{E}_m(t,z)|^2 dz$): (a) $\Delta = 0.055\ c/n_0L$, and (b) $\Delta = -0.055\ c/n_0L$, when several modes are initially excited.

In Fig. 3, we see that, under a constant effective force corresponding to a constant detuning Δ, the total intensity oscillates around the $m = 0$ point in the frequency axis. Next, we show that by varying the direction of the effective force periodically in time, as can be achieved by varying the detuning Δ periodically in time, we can achieve a unidirectional transport of light in the frequency space. In the simulation, we periodically switch Δ between $\pm 0.055\ c/n_0L$ at every time interval of $t = 55\ n_0L/c \sim \pi/|\Delta|$ [see Fig. 4(b)]. In the simulation we include 29 resonant modes ($m = -14, \ldots, 14$), to accommodate the range of frequency shift in the unidirectional transport process. The excitation follows Eqs. (13) and (14) with $\omega_c = \omega_{-12}$. In Fig. 4(a), we plot the total energy for each mode ($I_m(t)$). The Bloch oscillation is interrupted every time a sudden change in the modulation frequencies occurs, resulting in a unidirectional shift in the frequency space as a function of time.

In experiments, a ring is typically excited through the coupling to external waveguides. Here we demonstrate unidirectional frequency transport in the presence of external coupling waveguides (Fig. 5). We assume that the coupling occurs at a position at $z_{1,2}$ on the ring circumference with the external waveguide 1 or 2, as described by

$$\mathcal{E}_m(t^+, z_{1,2}) = \sqrt{1-\gamma_{1,2}^2(t)}\,\mathcal{E}_m(t^-, z_{1,2}) - i\gamma_{1,2}(t) E_m^{(1,2)}(t^-, z_{1,2}), \tag{15}$$

$$E_m^{(1,2)}(t^+, z_{1,2}) = \sqrt{1-\gamma_{1,2}^2(t)}\,E_m^{(1,2)}(t^-, z_{1,2}) - i\gamma_{1,2}(t)\mathcal{E}_m(t^-, z_{1,2}), \tag{16}$$

where $E_m^{(1,2)}$ is the amplitude of the field component at the frequency ω_m in external waveguide 1 or 2. $\gamma_{1,2}(t)$ is the coupling strength between the ring resonator and waveguide 1 or 2. For optimal observation of unidirectional transport along the frequency axis, it is preferable that the cavity does not leak into the waveguide during the modulation process. We therefore choose a time-dependent waveguide–cavity coupling constant in the form $\gamma_1(t) = 0.1H(40 - t)$ and $\gamma_2(t) = 0.1H(t - 200)$ in the simulation, where $H(t)$ is the Heaviside step function.

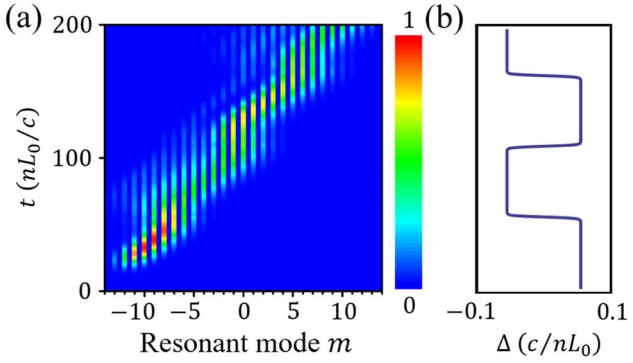

Fig. 4. (a) The evolution in time of the total energy for each resonant mode ($I_m(t)$), as the modulation frequency is periodically switched between $\Delta = \pm 0.055\ c/n_0L$, as described in (b).

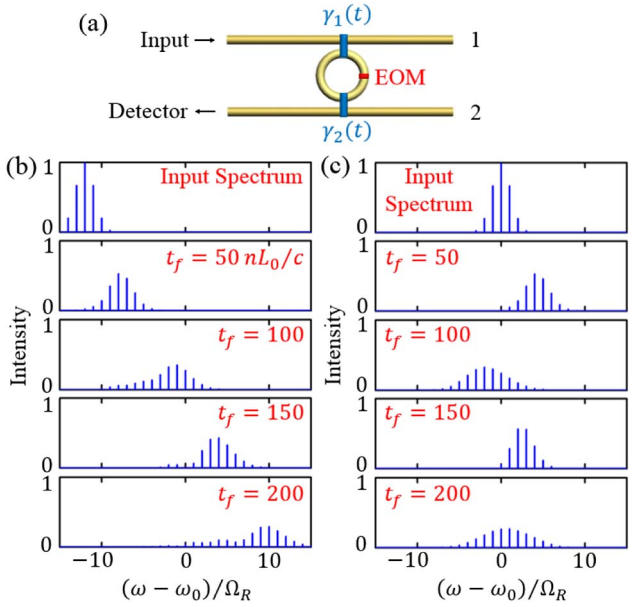

Fig. 5. (a) Ring resonator under dynamic modulation by the electro-optic modulator (EOM), and in addition coupled to two external waveguides. (b) and (c) Detected signals in external waveguide 2: the top panels are the input spectra injected through external waveguide 1. The ring is modulated for a period from 0 to t_f. The output spectra, after the modulation is turned off, are plotted in the remaining panels. In (b), the modulation frequency periodically switched between $\Delta = \pm 0.055\ c/n_0L$ as described in Fig. 4(b). In (c), the modulation frequency is maintained constant at $\Delta = 0.055\ c/n_0L$.

Such an on–off behavior in coupling can be achieved with electro-optic tuning of waveguide coupler [32]. With such a choice, the input source is injected into the ring from waveguide 1 at $t < 40\ n_0L/c$, and, after modulation, the field in the ring leaks out into waveguide 2 at $t > 200\ n_0L/c$ and gets detected. We first perform the simulation with the input field into external waveguide 1 obeying Eqs. (13) and (14) with $\omega_c = \omega_{-12}$. We turn on the dynamic modulation at $t = 0$ with the same periodic switch of the modulation frequency following Fig. 4(b), but turn it off at various times t_f ($t_f = 50, 100, 150, 200\ n_0L/c$). In Fig. 5(b), we plot the output spectrum from external waveguide 2 after the modulation is switched off. The top panel of Fig. 5(b) shows the profile of the input spectrum. Compared to it, the output spectra shift to higher frequencies. As t_f gets larger, the magnitude of the shift becomes larger, demonstrating the unidirectional frequency shift in this system. In contrast, in Fig. 5(c), we choose the same input field except $\omega_c = \omega_0$ in Eq. (14), and we apply a constant modulation frequency with $\Delta = 0.055\ c/n_0L$ instead over the same periods from 0 to the various t_f, as discussed above. For all values of t_f, the output spectra are located somewhat near ω_0, and do not exhibit the unidirectional shift as we observe in Fig. 5(b).

4. DISCUSSION AND CONCLUSION

We discuss a few experimental aspects for on-chip implementation of our theoretical predictions. Modulation-induced coupling between different resonant modes separated by a free spectral range was demonstrated in [31], which used a silicon ring resonator with a radius of 445 μm modulated at a frequency of $\Omega = 26$ GHz. Our theory can be implemented in a similar system. The maximum coupling strength between the modes, as observed in Ref. [31], translates to $\alpha \approx 0.8$ in Eq. (11) as applied to this system. Therefore, our choice of $\alpha = 0.2$ in the simulation is within what one can accomplish experimentally. To observe a period of Bloch oscillation, the photon lifetime τ_p in the ring needs to be larger than the period of a single Bloch oscillation $2\pi/\Delta$, which, with a choice of $\Delta \approx 0.1\Omega_R \approx 2$ GHz, translates into a requirement of the quality factor of the ring of the order of 10^5–10^6. Such a quality factor may be achievable in silicon ring modulators [31]. Alternatively, one can consider other material systems that have significant electro-optic effects, and where high-Q resonators have already been achieved [36]. To demonstrate the Hamiltonian of Eq. (2), there needs to be sufficient bandwidth over which the group velocity dispersion is small. For a silicon waveguide, near-zero group velocity dispersion has been observed over a bandwidth of 670 nm [37], which is far larger than what we require here.

Our study in general points to interesting opportunities for the control of light spectra through the use of dynamic modulation inside the cavity. While the simulation above is for a classical wave, since the phase modulator as described by Eq. (8) is a linear and lossless device, the same physics should occur in the quantum regime at the few photon level, as well. The unidirectional shift here is, therefore, potentially useful for photon frequency translation [27]. Importantly, here the magnitude of frequency translation can be far larger than the modulation frequency. Our work here also indicates other interesting new opportunities for manipulating the spectrum of light in microring resonators. For example, with a different choice of parameters, an effect of dynamic localization [29,35,38,39] in the frequency domain may be achieved. Our work here points to interesting new opportunities for manipulating the spectrum of light in microring resonators.

Funding. Air Force Office of Scientific Research (AFOSR) (FA9550-12-1-0488).

REFERENCES

1. K. J. Vahala, "Optical microcavities," Nature **424**, 839–846 (2003).
2. Q. Xu, S. Sandhu, M. L. Povinelli, J. Shakya, S. Fan, and M. Lipson, "Experimental realization of an on-chip all-optical analogue to electromagnetically induced transparency," Phys. Rev. Lett. **96**, 123901 (2006).
3. A. B. Matsko, A. A. Savchenkov, W. Liang, V. S. Ilchenko, D. Seidel, and L. Maleki, "Collective emission and absorption in a linear resonator chain," Opt. Express **17**, 15210–15215 (2009).
4. T. Hu, P. Yu, C. Qiu, H. Qiu, F. Wang, M. Yang, X. Jiang, H. Yu, and J. Yang, "Tunable Fano resonances based on two-beam interference in microring resonator," Appl. Phys. Lett. **102**, 011112 (2013).
5. B. Peng, S. K. Özdemir, F. Lei, F. Monifi, M. Gianfreda, G. L. Long, S. Fan, F. Nori, C. M. Bender, and L. Yang, "Parity-time-symmetric whispering-gallery microcavities," Nat. Phys. **10**, 394–398 (2014).
6. T. J. Kippenberg, R. Holzwarth, and S. A. Diddams, "Microresonator-based optical frequency combs," Science **332**, 555–559 (2011).
7. K. Saha, Y. Okawachi, J. S. Levy, R. K. W. Lau, K. Luke, M. A. Foster, M. Lipson, and A. L. Gaeta, "Broadband parametric frequency comb generation with a 1-μm pump source," Opt. Express **20**, 26935–26941 (2012).
8. S.-W. Huang, H. Zhou, J. Yang, J. F. McMillan, A. Matsko, M. Yu, D.-L. Kwong, L. Maleki, and C. W. Wong, "Mode-locked ultrashort pulse generation from on-chip normal dispersion microresonators," Phys. Rev. Lett. **114**, 053901 (2015).

9. A. R. Johnson, Y. Okawachi, M. R. E. Lamont, J. S. Levy, M. Lipson, and A. L. Gaeta, "Microresonator-based comb generation without an external laser source," Opt. Express **22**, 1394–1401 (2014).
10. S. B. Papp, K. Beha, P. Del'haye, F. Quinlan, H. Lee, K. J. Vahala, and S. A. Diddams, "Microresonator frequency comb optical clock," Optica **1**, 10–14 (2014).
11. A. G. Griffith, R. K. W. Lau, J. Cardenas, Y. Okawachi, A. Mohanty, R. Fain, Y. H. D. Lee, M. Yu, C. T. Phare, C. B. Poitras, A. L. Gaeta, and M. Lipson, "Silicon-chip mid-infrared frequency comb generation," Nat. Commun. **6**, 6299 (2015).
12. J. N. Winn, S. Fan, J. D. Joannopoulos, and E. P. Ippen, "Interband transitions in photonic crystals," Phys. Rev. B **59**, 1551–1554 (1999).
13. P. Dong, S. F. Preble, J. T. Robinson, S. Manipatruni, and M. Lipson, "Inducing photonic transitions between discrete modes in a silicon optical microcavity," Phys. Rev. Lett. **100**, 033904 (2008).
14. Z. Yu and S. Fan, "Complete optical isolation created by indirect interband photonic transitions," Nat. Photonics **3**, 91–94 (2009).
15. T. Ozawa, H. M. Price, N. Goldman, O. Zilberberg, and I. Carusotto, "Synthetic dimensions in integrated photonics: From optical isolation to four-dimensional quantum Hall physics," Phys. Rev. A **93**, 043827 (2016).
16. L. Yuan, Y. Shi, and S. Fan, "Photonic gauge potential in a system with a synthetic frequency dimension," Opt. Lett. **41**, 741–744 (2016).
17. G. Lenz, I. Talanina, and C. M. de Sterke, "Bloch oscillations in an array of curved optical waveguides," Phys. Rev. Lett. **83**, 963–966 (1999).
18. H. Trompeter, W. Krolikowski, D. N. Neshev, A. S. Desyatnikov, A. A. Sukhorukov, Y. S. Kivshar, T. Pertsch, U. Peschel, and F. Lederer, "Bloch oscillations and Zener tunneling in two-dimensional photonic lattices," Phys. Rev. Lett. **96**, 053903 (2006).
19. S. Longhi, "Optical Zener-Bloch oscillations in binary waveguide arrays," Europhys. Lett. **76**, 416–421 (2006).
20. F. Dreisow, A. Szameit, M. Heinrich, T. Pertsch, S. Nolte, A. Tünnermann, and S. Longhi, "Bloch-Zener oscillations in binary superlattices," Phys. Rev. Lett. **102**, 076802 (2009).
21. M. Levy and P. Kumar, "Nonreciprocal Bloch oscillations in magneto-optic waveguide arrays," Opt. Lett. **35**, 3147–3149 (2010).
22. U. Peschel, C. Bersch, and G. Onishchukov, "Discreteness in time," Open Phys. **6**, 619–627 (2008).
23. C. Bersch, G. Onishchukov, and U. Peschel, "Experimental observation of spectral Bloch oscillations," Opt. Lett. **34**, 2372–2374 (2009).
24. F. Bloch, "Über die Quantenmechanik der Elektronen in Kristallgittern," Z. Phys. **52**, 555–600 (1929).
25. E. Haller, R. Hart, M. J. Mark, J. G. Danzl, L. Reichsöllner, and H.-C. Nägerl, "Inducing transport in a dissipation-free lattice with super Bloch oscillations," Phys. Rev. Lett. **104**, 200403 (2010).
26. M. T. Rakher, L. Ma, O. Slattery, X. Tang, and K. Srinivasan, "Quantum transduction of telecommunications-band single photons from a quantum dot by frequency upconversion," Nat. Photonics **4**, 786–791 (2010).
27. H. J. McGuinness, M. G. Raymer, C. J. McKinstrie, and S. Radic, "Quantum frequency translation of single-photon states in a photonic crystal fiber," Phys. Rev. Lett. **105**, 093604 (2010).
28. P. Lodahl, S. Mahmoodian, and S. Stobbe, "Interfacing single photons and single quantum dots with photonic nanostructures," Rev. Mod. Phys. **87**, 347–400 (2015).
29. L. Yuan and S. Fan, "Three-dimensional dynamic localization of light from a time-dependent effective gauge field for photons," Phys. Rev. Lett. **114**, 243901 (2015).
30. N. W. Ashcroft and N. D. Mermin, *Solid State Physics* (Saunders College, 1976).
31. L. D. Tzuang, M. Soltani, Y. H. D. Lee, and M. Lipson, "High RF carrier frequency modulation in silicon resonators by coupling adjacent free-spectral-range modes," Opt. Lett. **39**, 1799–1802 (2014).
32. H. A. Haus, *Waves and Fields in Optoelectronics* (Prentice-Hall, 1984).
33. B. E. A. Saleh and M. C. Teich, *Fundamentals of Photonics*, 2nd ed. (Wiley, 2007).
34. H. A. Haus, "Mode-locking of lasers," IEEE J. Sel. Top. Quantum Electron. **6**, 1173–1185 (2000).
35. D. H. Dunlap and V. M. Kenkre, "Dynamic localization of a charged particle moving under the influence of an electric field," Phys. Rev. B **34**, 3625–3633 (1986).
36. A. A. Savchenkov, A. B. Matsko, V. S. Ilchenko, I. Solomatine, D. Seidel, and L. Maleki, "Tunable optical frequency comb with a crystalline whispering gallery mode resonator," Phys. Rev. Lett. **101**, 093902 (2008).
37. L. Zhang, Q. Lin, Y. Yue, Y. Yan, R. G. Beausoleil, and A. E. Willner, "Silicon waveguide with four zero-dispersion wavelengths and its application in on-chip octave-spanning supercontinuum generation," Opt. Express **20**, 1685–1690 (2012).
38. S. Longhi, "Self-imaging and modulational instability in an array of periodically curved waveguides," Opt. Lett. **30**, 2137–2139 (2005).
39. A. Joushaghani, R. Iyer, J. K. S. Poon, J. S. Aitchison, C. M. de Sterke, J. Wan, and M. M. Dignam, "Generalized exact dynamic localization in curved coupled optical waveguide arrays," Phys. Rev. Lett. **109**, 103901 (2012).